BULLETIN OF THE BRAZILIAN MATHEMATICAL SOCIETY

Bull Braz Math Soc, New Series 47(1), 91-103

ISSN: 1678-7544 (Print) / 1678-7714 (Online)

Central-upwind scheme for shallow water equations with discontinuous bottom topography

Andrew Bernstein, Alina Chertock and Alexander Kurganov*

Abstract. Finite-volume central-upwind schemes for shallow water equations were proposed in [A. Kurganov and G. Petrova, Commun. Math. Sci., **5** (2007), 133–160]. These schemes are capable of maintaining "lake-at-rest" steady states and preserving the positivity of the computed water depth. The well-balanced and positivity preserving features of the central-upwind schemes are achieved, in particular, by using continuous piecewise linear interpolation of the bottom topography function. However, when the bottom function is discontinuous or a model with a moving bottom topography is studied, the continuous piecewise linear approximation may not be sufficiently accurate and robust.

In this paper, we modify the central-upwind scheme by approximating the bottom topography function using a discontinuous piecewise linear reconstruction (the same approximation used to reconstruct evolved quantities in the finite-volume setting) as well as implementing a special quadrature for the geometric source term and draining time step technique. We prove that the new central-upwind scheme possesses the well-balanced and positivity preserving properties and illustrate its performance on a number of numerical examples.

Keywords: hyperbolic system of conservation and balance laws, semi-discrete central-upwind scheme, Saint Venant system of shallow water equations.

Mathematical subject classification: 76M12, 65M08, 35L65, 86-08, 86A05.

1 Introduction

In this paper, we are interested in solving the one-dimensional (1-D) Saint-Venant system of shallow water equations introduced in [6] and still widely used

Received 6 April 2015.
*Corresponding author.

in modeling flows in rivers, lakes and coastal areas as well as atmospheric and oceanic flows in certain regimes. The 1-D Saint-Venant system reads as follows:

$$\begin{pmatrix} h \\ hu \end{pmatrix}_t + \begin{pmatrix} hu \\ hu^2 + \frac{g}{2}h^2 \end{pmatrix}_x = \begin{pmatrix} 0 \\ -ghB_x \end{pmatrix}, \tag{1.1}$$

where $B(x)$ is the bottom topography elevation, $h(x,t)$ is the fluid depth above the bottom, $u(x,t)$ is the velocity, and g is the gravitational constant.

When solving the system of balance laws (1.1) numerically, one typically faces several difficulties. One difficulty stems from the fact that many physically relevant solutions of (1.1) are small perturbations of steady-state solutions. Therefore, if a delicate balance between the flux and geometric source term in the second equation in (1.1) is not respected, the solution may develop spurious waves of a magnitude that can become larger than the exact solution. A second numerical challenge is when the water depth h is very small. In this regime, even small numerical oscillation in the computed solution can result in a negative computed h value, which is not only physically irrelevant, but also cause the numerical scheme to break down since the eigenvalues of the Jacobian of (1.1) are $u \pm \sqrt{gh}$.

To overcome these numerical challenges, one needs to use a scheme that is both well-balanced and positivity preserving. We start by noting that the system (1.1) has a family of smooth steady-state solutions given by:

$$q := hu \equiv \text{Const}, \quad \frac{u^2}{2} + g(h+B) \equiv \text{Const}. \tag{1.2}$$

The most practically important steady-state solutions among (1.2) are the "lake-at-rest" solutions characterized by:

$$q = 0, \quad w := h + B = \text{Const}, \tag{1.3}$$

where w is the water surface. We will call the scheme well-balanced if it is capable of exactly preserving equilibrium variables q and w in (1.3) at the discrete level.

A number of well-balanced and positivity preserving numerical methods have been proposed in the literature, see, e.g., [1, 2, 3, 4, 12, 17]. In particular, central-upwind schemes, proposed in [12], are Riemann-problem-solver-free Godunov type methods originally developed in [10, 11, 13] for general multidimensional hyperbolic systems of conservation laws. The central-upwind scheme in [12] is well-balanced and positivity preserving thanks to several special techniques, including a continuous piecewise linear approximation of the bottom topography function B. Though the scheme in [12] is quite robust, its accuracy

may deteriorate when B is not smooth, in which case the continuous interpolation of B may prevent the scheme from achieving high resolution. Moreover, enforcing continuity of B may create difficulties when the central-upwind scheme is extended to models with moving, time-dependent bottom topography function B (studying of such models is out of scope of the current paper).

In this paper, we introduce a modified version of the second-order semi-discrete central-upwind scheme from [12]. The new scheme relies on a *discontinuous* piecewise linear reconstruction of the bottom topography function B and thus is suitable for functions B containing large jumps. The well-balanced feature of the new scheme is guaranteed by a special numerical quadrature used for approximating the geometrical source term in the right-hand side (RHS) of the system (1.1). The quadrature is similar to the one proposed in [9] in the context of compressible two-phase flows. The positivity of the computed water depth is achieved by applying a draining time step technique from in [3]. We illustrate the performance of the introduced central-upwind scheme on a number of numerical examples.

2 Modified Central-Upwind Scheme

Following [12], we start by rewriting the system (1.1) in terms of the equilibrium variables $\boldsymbol{U} = (w, q)^T$:

$$\begin{pmatrix} w \\ q \end{pmatrix}_t + \begin{pmatrix} q \\ qu + \dfrac{g}{2}(w^2 - 2wB) \end{pmatrix}_x = \begin{pmatrix} 0 \\ -gwB_x \end{pmatrix}. \tag{2.1}$$

We introduce a uniform grid $x_\alpha := \alpha\Delta x$, with a finite volume cell denoted by $I_j := [x_{j-\frac{1}{2}}, x_{j+\frac{1}{2}}]$, in which a cell average of the computed solution, $\overline{\boldsymbol{U}}_j(t) \approx \dfrac{1}{\Delta x}\displaystyle\int_{I_j} \boldsymbol{U}(x,t)dx$, is assumed to be known at a given time t. The cell averages are evolved in time based on the following equation:

$$\frac{d}{dt}\overline{\boldsymbol{U}}_j(t) = -\frac{\boldsymbol{H}_{j+\frac{1}{2}}(t) - \boldsymbol{H}_{j-\frac{1}{2}}(t)}{\Delta x} + \overline{\boldsymbol{S}}_j(t), \tag{2.2}$$

where $\boldsymbol{H}_{j+\frac{1}{2}}$ are the numerical fluxes and

$$\overline{\boldsymbol{S}}_j(t) \approx \frac{1}{\Delta x}\int_{I_j} \boldsymbol{S}(\boldsymbol{U}, B)dx \tag{2.3}$$

are the cell averages of the geometric source term $\boldsymbol{S} = (0, -gwB_x)^T$. For the rest of this paper we will drop the notation t for time dependence for simplicity where it is appropriate.

The construction of the scheme will be complete once the numerical fluxes $\boldsymbol{H}_{j+\frac{1}{2}}$ in (2.4) and the source term $\overline{\boldsymbol{S}}_j$ in (2.3) are computed so that the resulting method is well-balanced and positivity preserving.

Numerical Fluxes. In (2.2), we use the central-upwind numerical fluxes from [11]:

$$\begin{aligned}\boldsymbol{H}_{j+\frac{1}{2}}(t) = &\frac{a^+_{j+\frac{1}{2}}\boldsymbol{F}\left(\boldsymbol{U}^-_{j+\frac{1}{2}}, B^-_{j+\frac{1}{2}}\right) - a^-_{j+\frac{1}{2}}\boldsymbol{F}\left(\boldsymbol{U}^+_{j+\frac{1}{2}}, B^+_{j+\frac{1}{2}}\right)}{a^+_{j+\frac{1}{2}} - a^-_{j+\frac{1}{2}}}\\ &+\frac{a^+_{j+\frac{1}{2}}a^-_{j+\frac{1}{2}}}{a^+_{j+\frac{1}{2}} - a^-_{j+\frac{1}{2}}}\left[\boldsymbol{U}^+_{j+\frac{1}{2}} - \boldsymbol{U}^-_{j+\frac{1}{2}}\right]\end{aligned} \tag{2.4}$$

with $\boldsymbol{F}(\boldsymbol{U}, B) := \left(q, qu + \frac{g}{2}(w^2 - 2wB)\right)^T$.

Reconstruction. In equation (2.4), $\boldsymbol{U}^{\pm}_{j+\frac{1}{2}}$ are the left and right point values of the piecewise linear reconstructions

$$\widetilde{\boldsymbol{U}}(x) = \sum_j \left[\overline{\boldsymbol{U}}_j + (\boldsymbol{U}_x)_j(x - x_j)\right]\cdot \chi_{I_j}(x) \tag{2.5}$$

obtained at cell interfaces $x = x_{j+\frac{1}{2}}$ by

$$\boldsymbol{U}^+_{j+\frac{1}{2}} = \overline{\boldsymbol{U}}_{j+1} - \frac{\Delta x}{2}(\boldsymbol{U}_x)_{j+1}, \quad \boldsymbol{U}^-_{j+\frac{1}{2}} = \overline{\boldsymbol{U}}_j + \frac{\Delta x}{2}(\boldsymbol{U}_x)_j. \tag{2.6}$$

In (2.5) and (2.6), $\chi_{I_j}(x)$ is the characteristic function of the interval I_j and $(\mathbf{U}_x)_j$ are the numerical derivatives, which should be computed using a nonlinear limiter in order to minimize oscillations. In our numerical experiments, we use the generalized minmod limiter (see, e.g., [15, 16, 18, 19]):

$$\begin{aligned}&(\boldsymbol{U}_x)_j =\\ &\text{minmod}\left(\theta\frac{\overline{\boldsymbol{U}}_j - \overline{\boldsymbol{U}}_{j-1}}{\Delta x}, \frac{\overline{\boldsymbol{U}}_{j+1} - \overline{\boldsymbol{U}}_{j-1}}{2\Delta x}, \theta\frac{\overline{\boldsymbol{U}}_{j+1} - \overline{\boldsymbol{U}}_j}{\Delta x}\right), \quad \theta \in [1, 2],\end{aligned} \tag{2.7}$$

where the minmod function is defined by

$$\text{minmod}(z_1, z_2, \ldots) := \begin{cases}\min_j\{z_j\}, & \text{if } z_j > 0 \ \ \forall j,\\ \max_j\{z_j\}, & \text{if } z_j < 0 \ \ \forall j,\\ 0, & \text{otherwise.}\end{cases} \tag{2.8}$$

The parameter θ in (2.7) is used to control the amount of the numerical viscosity, with large θ values resulting in less dissipative results.

Piecewise Linear Approximation of B. Unlike the original central-upwind scheme in [12], where the bottom topography function B was replaced with a continuous piecewise linear approximation, here we approximate B by using the same generically discontinuous piecewise linear reconstruction

$$\widetilde{B}(x) = \sum_j \Big[B(x_j) + (B_x)_j(x - x_j)\Big] \cdot \chi_{I_j}(x) \tag{2.9}$$

to obtain the point values $B^{\pm}_{j+\frac{1}{2}}$ at $x = x_{j+\frac{1}{2}}$:

$$B^{+}_{j+\frac{1}{2}} = \overline{B}_{j+1} - \frac{\Delta x}{2}(B_x)_{j+1}, \quad B^{-}_{j+\frac{1}{2}} = \overline{B}_j + \frac{\Delta x}{2}(B_x)_j. \tag{2.10}$$

Positivity Correction for $\widetilde{w}$. When $\widetilde{w}$ is reconstructed using (2.5), some of the point values $w^{\pm}_{j\pm\frac{1}{2}}$, obtained in (2.6), may be smaller than the corresponding values $B^{\pm}_{j\pm\frac{1}{2}}$, which would lead to negative point values of h. We therefore follow [12] and correct the reconstruction of $\widetilde{w}$ according to the following simple algorithm:

$$\text{if } w^{-}_{j+\frac{1}{2}} < B^{-}_{j+\frac{1}{2}}, \text{ then take } (w_x)_j := \frac{B^{-}_{j+\frac{1}{2}} - \overline{w}_j}{\Delta x/2}$$

$$\Longrightarrow w^{-}_{j+\frac{1}{2}} = B^{-}_{j+\frac{1}{2}}, \quad w^{+}_{j-\frac{1}{2}} = 2\overline{w}_j - B^{-}_{j+\frac{1}{2}}, \tag{2.11}$$

$$\text{if } w^{+}_{j-\frac{1}{2}} < B^{+}_{j-\frac{1}{2}}, \text{ then take } (w_x)_j := \frac{\overline{w}_j - B^{+}_{j-\frac{1}{2}}}{\Delta x/2}$$

$$\Longrightarrow w^{-}_{j+\frac{1}{2}} = 2\overline{w}_j - B^{+}_{j-\frac{1}{2}}, \quad w^{+}_{j-\frac{1}{2}} = B_{j-\frac{1}{2}}. \tag{2.12}$$

Notice that this correction algorithm works as long as $\overline{w}_j > \overline{B}_j$.

After the values $w^{\pm}_{j+\frac{1}{2}}$ are corrected, we compute the point values of the water depth as follows:

$$h^{\pm}_{j+\frac{1}{2}} := w^{\pm}_{j+\frac{1}{2}} - B^{\pm}_{j+\frac{1}{2}}. \tag{2.13}$$

Velocity Desingularization. In order to avoid division by zero (or by a very small number), we desingularize the computation of the velocity point values needed in (2.4) by setting

$$u^{\pm}_{j+\frac{1}{2}} = \frac{2h^{\pm}_{j+\frac{1}{2}} q^{\pm}_{j+\frac{1}{2}}}{\big(h^{\pm}_{j+\frac{1}{2}}\big)^2 + \max\Big[\big(h^{\pm}_{j+\frac{1}{2}}\big)^2, \varepsilon^2\Big]}, \tag{2.14}$$

where ε is a small desingularization parameter (in all of our numerical examples, we have used $\varepsilon = 10^{-5}$). For more details on different desingularization strategies, see the discussions in [5, 12].

For consistency, the desingularized velocities should be used to modify the corresponding values of the discharge by

$$q^{\pm}_{j+\frac{1}{2}} = h^{\pm}_{j+\frac{1}{2}} \cdot u^{\pm}_{j+\frac{1}{2}}.$$

Local Speeds. The one-sided local speed of propagation $a^{\pm}_{j+\frac{1}{2}}$ used in the central-upwind numerical flux (2.4) are obtained using the largest and smallest eigenvalues of the Jacobian of (1.1) and are given by

$$\begin{aligned} a^{+}_{j+\frac{1}{2}} &= \max\left\{u^{+}_{j+\frac{1}{2}} + \sqrt{gh^{+}_{j+\frac{1}{2}}},\ u^{-}_{j+\frac{1}{2}} + \sqrt{gh^{-}_{j+\frac{1}{2}}},\ 0\right\},\\ a^{-}_{j+\frac{1}{2}} &= \min\left\{u^{+}_{j+\frac{1}{2}} - \sqrt{gh^{+}_{j+\frac{1}{2}}},\ u^{-}_{j+\frac{1}{2}} - \sqrt{gh^{-}_{j+\frac{1}{2}}},\ 0\right\}. \end{aligned} \tag{2.15}$$

Well-Balanced Quadrature for the Geometric Source Terms. In order to ensure the method is well-balanced a special quadrature should be used to discretize the second component $\overline{S}^{(2)}_j$ of the source term in (2.3). A proper discretization should guarantee that the RHS of (2.2) vanishes at at "lake-at-rest" steady states, at which $q^{\pm}_{j+\frac{1}{2}} = q^{\pm}_{j-\frac{1}{2}} = 0$, $w^{\pm}_{j+\frac{1}{2}} = w^{\pm}_{j-\frac{1}{2}} = \overline{w}_j$, and thus

$$\begin{aligned} &\frac{H^{(2)}_{j-\frac{1}{2}} - H^{(2)}_{j+\frac{1}{2}}}{\Delta x}\\ &= \frac{g\overline{w}_j}{\Delta x}\left(\frac{a^{+}_{j+\frac{1}{2}}B^{-}_{j+\frac{1}{2}} - a^{-}_{j+\frac{1}{2}}B^{+}_{j+\frac{1}{2}}}{a^{+}_{j+\frac{1}{2}} - a^{-}_{j+\frac{1}{2}}} - \frac{a^{+}_{j-\frac{1}{2}}B^{-}_{j-\frac{1}{2}} - a^{-}_{j-\frac{1}{2}}B^{+}_{j-\frac{1}{2}}}{a^{+}_{j-\frac{1}{2}} - a^{-}_{j-\frac{1}{2}}}\right). \end{aligned}$$

Therefore the RHS of (2.2) is equal to zero if the source term is discretized as follows:

$$\overline{S}^{(2)}_j \approx -\frac{g\overline{w}_j}{\Delta x}\left(\frac{a^{+}_{j+\frac{1}{2}}B^{-}_{j+\frac{1}{2}} - a^{-}_{j+\frac{1}{2}}B^{+}_{j+\frac{1}{2}}}{a^{+}_{j+\frac{1}{2}} - a^{-}_{j+\frac{1}{2}}} - \frac{a^{+}_{j-\frac{1}{2}}B^{-}_{j-\frac{1}{2}} - a^{-}_{j-\frac{1}{2}}B^{+}_{j-\frac{1}{2}}}{a^{+}_{j-\frac{1}{2}} - a^{-}_{j-\frac{1}{2}}}\right). \tag{2.16}$$

Time Evolution. The central-upwind semi-discretization (2.2) is a system of ODEs, which should be integrated by a sufficiently accurate and stable ODE solver. We first note that the bottom topography function B is independent of

time and therefore the forward Euler time step for the first component in (2.2) can be written in the following form:

$$\overline{h}_j^{n+1} = \overline{h}_j^n - \frac{\Delta t}{\Delta x}\left(H^{(1)}_{j+\frac{1}{2}} - H^{(1)}_{j-\frac{1}{2}}\right), \tag{2.17}$$

where Δt is the time step constrained by the CFL condition (see [12])

$$\frac{\Delta t}{\Delta x}\max_j \left|a^{\pm}_{j\pm\frac{1}{2}}\right| \le \frac{1}{2}. \tag{2.18}$$

In order to guarantee the positivity of $\overline{h}_j^{n+1}$ provided $\overline{h}_j^n \ge 0\ \forall j$, we adopt a draining time-step technique from [4, 3]. To this end, we introduce the draining time step

$$\Delta t_j^{drain} := \frac{\Delta x\, \overline{h}_j^n}{\max\left(0, H^{(1)}_{j+\frac{1}{2}}\right) + \max\left(0, -H^{(1)}_{j-\frac{1}{2}}\right)}, \tag{2.19}$$

which describes the time when the water contained in cell I_j in the beginning of the time step has left via the outflow fluxes. We now replace the evolution step in (2.17) by:

$$\overline{h}_j^{n+1} = \overline{h}_j^n - \frac{\Delta t_{j+\frac{1}{2}} H^{(1)}_{j+\frac{1}{2}} - \Delta t_{j-\frac{1}{2}} H^{(1)}_{j-\frac{1}{2}}}{\Delta x}, \tag{2.20}$$

where the time step $\Delta t_{j+\frac{1}{2}}$ is defined as:

$$\Delta t_{j+\frac{1}{2}} = \min\left(\Delta t, \Delta t_i^{drain}\right), \quad i = j + \frac{1}{2} - \frac{\operatorname{sgn}\left(H^{(1)}_{j+\frac{1}{2}}\right)}{2}, \tag{2.21}$$

with Δt satisfying (2.18). Thus, we have $\overline{h}_j^{n+1} \ge 0,\ \forall j$ in our new scheme by construction.

A higher-order time discretization can be obtained using strong stability preserving (SSP) ODE solvers, which can be represented as a convex combination of forward Euler time steps, see, e.g., [7, 8]. Positivity preserving SSP methods are thus obtained by replacing the forward Euler steps (2.17) with the modified ones (2.20). In all of our numerical experiments, we used a modified version of the third-order SSP Runge-Kutta method.

3 Numerical Examples

In this section, we present three numerical examples. In all of the numerical simulations, the bottom topography is reconstructed according to (2.9) with

$(B_x)_j$ computed using the minmod limiter with $\theta = 1$. The equilibrium variables w and q are reconstructed using the minmod limiter with either $\theta = 1.3$ (Examples 1 and 2) or $\theta = 1$ (Example 3, in which we select the most diffusive version of the limiter to limit the oscillations). In all of the examples below, we use absorbing boundary conditions on both ends of the domain.

Example 1 – Small Perturbation of Steady State. In this problem, taken from [12], we study propagation of a small perturbation of the steady-state solution that contains nearly dry areas. The computational domain is $[-1, 1]$, the gravitational constant $g = 1$, the initial data are

$$w(x,0) = \begin{cases} 1.001, & 0.1 \le x \le 0.2, \\ 1, & \text{otherwise}, \end{cases} \qquad u(x,0) \equiv 0,$$

and the bottom topography is given by

$$B(x) = \begin{cases} 10(x-0.3), & 0.3 \le x \le 0.4, \\ 1 - 0.0025\sin^2(25\pi(x-0.4)), & 0.4 \le x \le 0.6, \\ -10(x-0.7), & 0.6 \le x \le 0.7, \\ 0, & \text{otherwise}. \end{cases}$$

A small perturbation of the "lake-at-rest" steady state initially located at $x \in [0.1, 0.2]$ is split into two parts propagating in the opposite directions. When the right-going wave propagates over the oscillating part of the bottom above which the initial water depth is very small ($x \in [0.4, 0.6]$), a complicated surface wave structure is developed. In Figure 3.1, we compare the solutions obtained by the proposed well-balanced central-upwind scheme and its non-well-balanced version, obtained by replacing the well-balanced quadrature (2.16) with the midpoint one,

$$\overline{S}_j^{(2)} \approx -g\overline{w}_j B_x(x_j),$$

and increasing the value of the desingularization parameter ε from 10^{-5} to 10^{-4} (the latter is needed to improve the efficiency of the non-well-balanced version of the scheme). Both solutions are computed until the final time $t = 1$ using $N = 400$ (top row) and $N = 1600$ (bottom row) uniform cells. As one can see, the non-well-balanced solution is very oscillatory and the magnitude of oscillations decrease quite slow when the mesh is refined. More details can be seen in Figure 3.1 (right column), where we zoom into the low water depth region $x \in [0.395, 0.5]$.

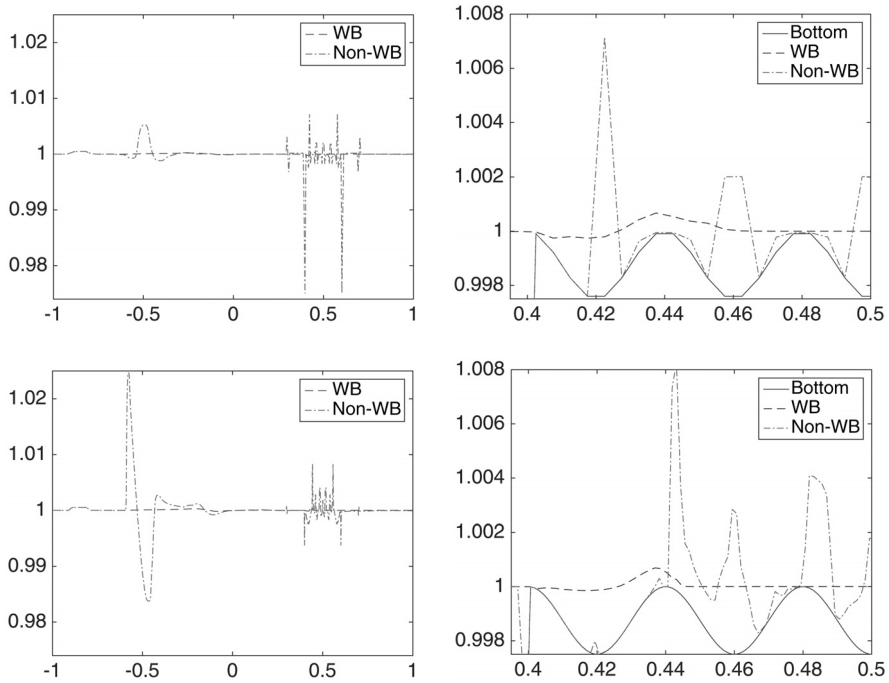

Figure 3.1: Example 1: Solution (w) computed by the well-balanced and non-well-balanced central upwind schemes using $N = 400$ (top row) and $N = 1600$ (bottom row) uniform cells. Right column: zoom into the region $x \in [0.395, 0.5]$.

Example 2 – Riemann Problem with Unique Solution. In this example, we consider the Riemann problem from [14, Test 7], where the system (1.1) is solved with $g = 9.8$ and the following Riemann data:

$$B(x) = \begin{cases} 1.1, & x < 0, \\ 1, & x > 0, \end{cases} \quad h(x,t) = \begin{cases} 1, & x < 0, \\ 0.8, & x > 0, \end{cases} \quad u(x,t) = \begin{cases} 2, & x < 0, \\ 4, & x > 0. \end{cases} \tag{3.1}$$

In [14], the exact solution of the initial value problem (IVP) (1.1), (3.1) was obtained and it was also shown that the Godunov-type scheme based on the exact solution of the Riemann problem fails at this test.

The central-upwind scheme proposed in this paper is, on the other hand, capable of accurately capturing the exact solution of the IVP (1.1), (3.1). To demonstrate this, we compute the numerical solution until the final time $t = 0.03$ on two uniform grids with $\Delta x = 0.004$ and 0.001 and compare the obtained solution with a reference one computed with $\Delta x = 0.00004$. We plot the

computed water depth h and velocity u in Figure 3.2, where one can clearly observe the convergence towards the reference solution, which agrees very well with the exact one (see [14, Test 7]).

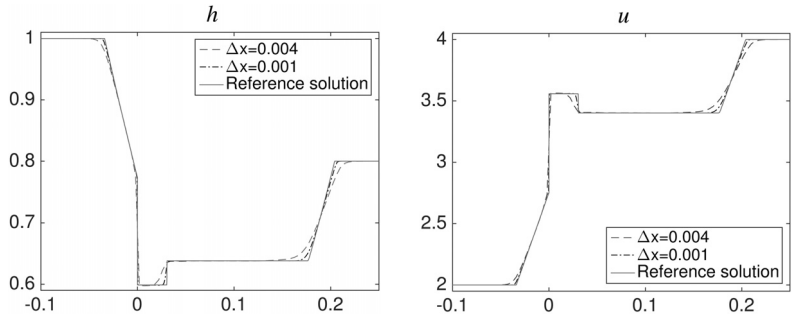

Figure 3.2: Example 2: Solution (h on the left and u on the right) computed using $\Delta x = 0.004$ and 0.001 and compared with the reference solution.

Example 3 – Riemann Problem with Multiple Solutions. In the final example, we consider the Riemann problem from [14, Test 6], where the system (1.1) is solved with $g = 9.8$ and different Riemann data:

$$B(x) = \begin{cases} 1, & x < 0, \\ 1.2, & x > 0, \end{cases} \qquad h(x,t) = \begin{cases} 0.2, & x < 0, \\ 0.75904946, & x > 0, \end{cases}$$
$$u(x,t) = \begin{cases} 5, & x < 0, \\ 1.3410741, & x > 0. \end{cases} \tag{3.2}$$

As it was shown in [14], the IVP (1.1), (3.2) admits three distinct analytic solution and Godunov-type upwind schemes based on different Riemann problem solvers converge to different analytic solutions. We compute the numerical solution until the final time $t = 0.1$ on three uniform grids with $\Delta x = 0.004$, 0.001 and 0.00004 using both the central-upwind scheme proposed in this paper and the central-upwind scheme from [12]. The results are plotted in Figures 3.3 and 3.4, respectively. As one can see, the schemes converge to different limits, each of which agrees well with the second and third analytic solutions from [14, Test 6].

Acknowledgment. The work of A. Bernstein was supported in part by the NSF Grant DMS-1216974. The work of A. Chertock was supported in part by the NSF Grant DMS-1216974 and the ONR Grant N00014-12-1-0832. The work of A. Kurganov was supported in part by the NSF Grant DMS-1216957 and the ONR Grant N00014-12-1-0833.

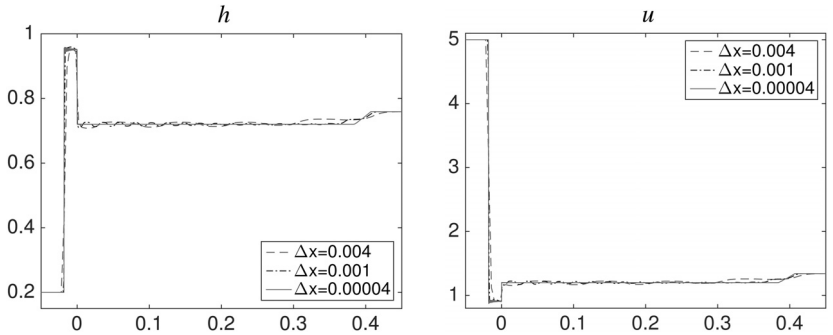

Figure 3.3: Example 3: Solution (h on the left and u on the right) computed by the proposed central-upwind scheme using $\Delta x = 0.004, 0.001$ and 0.00004.

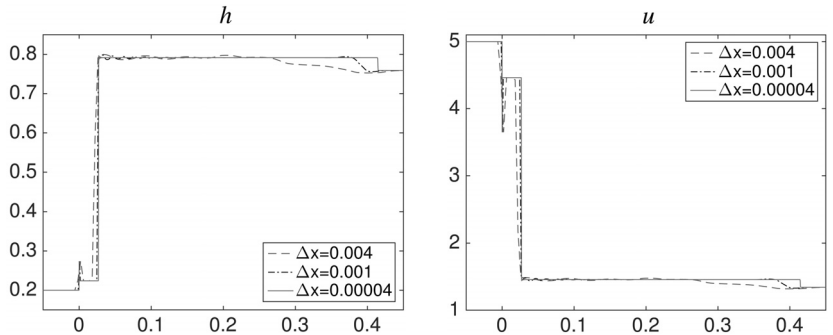

Figure 3.4: Example 3: Solution (h on the left and u on the right) computed by the central-upwind scheme from [12] using $\Delta x = 0.004, 0.001$ and 0.00004.

References

[1] E. Audusse, F. Bouchut, M.-O. Bristeau, R. Klein and B. Perthame. *A fast and stable well-balanced scheme with hydrostatic reconstruction for shallow water flows.* SIAM J. Sci. Comput., **25** (2004), 2050–2065.

[2] C. Berthon and F. Marche. *A positive preserving high order VFRoe scheme for shallow water equations: a class of relaxation schemes.* SIAM J. Sci. Comput., **30**(5) (2008), 2587–2612.

[3] A. Bollermann, G. Chen, A. Kurganov and S. Noelle. *A well-balanced reconstruction of wet/dry fronts for the shallow water equations.* J. Sci. Comput., **56**(2) (2013), 267–290.

[4] A. Bollermann, S. Noelle and M. Lukáčová-Medviďová. *Finite volume evolution Galerkin methods for the shallow water equations with dry beds.* Commun. Comput. Phys., **10**(2) (2011), 371–404.

[5] A. Chertock, S. Cui, A. Kurganov and T. Wu. *Well-balanced positivity preserving centralupwind scheme for the shallow water system with friction terms.* Internat. J. Numer. Meth. Fluids, Submitted.

[6] A.J.C. de Saint-Venant. *Thèorie du mouvement non-permanent des eaux, avec application aux crues des rivière at à l'introduction des marées dans leur lit.* C.R. Acad. Sci. Paris, **73** (1871), 147–154.

[7] S. Gottlieb, D. Ketcheson and C.-W. Shu. *Strong stability preserving Runge-Kutta and multistep time discretizations.* World Scientific Publishing Co. Pte. Ltd., Hackensack, NJ (2011).

[8] S. Gottlieb, C.-W. Shu and E. Tadmor. *Strong stability-preserving high-order time discretization methods.* SIAM Rev., **43** (2001), 89–112.

[9] A. Kurganov. *Well-balanced central-upwind scheme for compressible two-phase flows.* Proceedings of the European Conference on Computational Fluid Dynamics ECCOMAS CFD (2006).

[10] A. Kurganov and C.-T. Lin. *On the reduction of numerical dissipation in central-upwind schemes.* Commun. Comput. Phys., **2** (2007), 141–163.

[11] A. Kurganov, S. Noelle and G. Petrova. *Semi-discrete central-upwind scheme for hyperbolic conservation laws and Hamilton-Jacobi equations.* SIAM J. Sci. Comput., **23** (2001), 707–740.

[12] A. Kurganov and G. Petrova. *A second-order well-balanced positivity preserving centralupwind scheme for the saint-venant system.* Commun. Math. Sci., **5** (2007), 133–160.

[13] A. Kurganov and E. Tadmor. *New high resolution central schemes for non-linear conservation laws and convection-diffusion equations.* J. Comput. Phys., **160** (2000), 241–282.

[14] P.G. LeFloch and M.D. Thanh. *A Godunov-type method for the shallow water equations with discontinuous topography in the resonant regime.* Journal of Computational Physics, **230** (2011), 7631–7660.

[15] K.-A. Lie and S. Noelle. *On the artificial compression method for second-order nonoscillatory central difference schemes for systems of conservation laws.* SIAM J. Sci. Comput., **24**(4) (2003), 1157–1174.

[16] H. Nessyahu and E. Tadmor. *Nonoscillatory central differencing for hyperbolic conservation laws.* J. Comput. Phys., **87**(2) (1990), 408–463.

[17] B. Perthame and C. Simeoni. *A kinetic scheme for the Saint-Venant system with a source term.* Calcolo, **38**(4) (2001), 201–231.

[18] P.K. Sweby. *High resolution schemes using flux limiters for hyperbolic conservation laws.* SIAM J. Numer. Anal., **21**(5) (1984), 995–1011.

[19] B. van Leer. *Towards the ultimate conservative difference scheme. V. A second-order sequel to Godunov's method.* J. Comput. Phys., **32**(1) (1979), 101–136.

Andrew Bernstein and **Alina Chertock**
Department of Mathematics
North Carolina State University
Raleigh, NC, 27695
USA

E-mails: asbernst@ncsu.edu; chertock@math.ncsu.edu

Alexander Kurganov
Mathematics Department
Tulane University
New Orleans, LA 70118
USA

E-mail: kurganov@math.tulane.edu